

# NUCLEAR QUADRUPOLE SPIN–LATTICE RELAXATION IN $\text{Bi}_4\text{Ge}_3\text{O}_{12}$ SINGLE CRYSTALS DOPED WITH ATOMS OF $d$ OR $f$ ELEMENTS. CRYSTAL FIELD EFFECTS IN COMPOUNDS EXHIBITING ANOMALOUS MAGNETIC PROPERTIES

*V. G. Orlov<sup>a,b\*</sup>, G. S. Sergeev<sup>a,b</sup>, Tetsuo Asaji<sup>c</sup>, E. A. Kravchenko<sup>d</sup>, Yu. F. Kargin<sup>e</sup>*

<sup>a</sup>*Russian Research Center “Kurchatov Institute”  
123182, Moscow, Russia*

<sup>b</sup>*Moscow Institute for Physics and Technology (State University)  
117303, Moscow, Russia*

<sup>c</sup>*Department of Chemistry, College of Humanities and Sciences, Nihon University  
156-8550, Tokyo, Japan*

<sup>d</sup>*Institute of General and Inorganic Chemistry, Russian Academy of Sciences  
119991, Moscow, Russia*

<sup>e</sup>*State Institute of Metallurgy and Material Science, Russian Academy of Sciences  
119991, Moscow, Russia*

Received August 19, 2009

The nuclear quadrupole spin–lattice relaxation was studied in the range 4.2–300 K for single crystals of  $\text{Bi}_4\text{Ge}_3\text{O}_{12}$  doped with minor amounts (the tenth fractions of mol%) of paramagnetic atoms of Cr, Nd, and Gd. Unusual spin dynamic features were recently found for these crystals at room temperature: a dramatic (up to 8-fold) extension of the effective nuclear quadrupole spin–spin relaxation time  $T_2^*$  occurred upon doping the pure  $\text{Bi}_4\text{Ge}_3\text{O}_{12}$  sample. Unlike  $T_2^*$ , the effective spin–lattice relaxation time  $T_1^*$  at room temperature differs insignificantly for both doped and pure samples. But at lower temperatures, the samples exhibit considerably different behavior of the spin–lattice relaxation with temperature, which is caused by different contributions to the relaxation process of the dopant paramagnetic atoms. The distinctive maximum in the temperature dependence of the spin–lattice relaxation time for the Nd-doped crystal is shown to result from the crystal electric field effects.

## 1. INTRODUCTION

$\text{Bi}_4\text{Ge}_3\text{O}_{12}$  (BGO) belongs to the group of bismuth (III) oxide compounds of the general composition  $\text{Bi}_k\text{Al}_l\text{O}_m\text{X}_n$  ( $A = \text{Al, B, Ge, Ba}$  and  $X = \text{Cl, Br}$ ), some of which exhibit anomalous magnetic properties incompatible with their classification as diamagnetic compounds [1]. The results of computer modeling the  $^{209}\text{Bi}$  NQR Zeeman patterns [2] as well as spin echo envelope (SEE) modulations in BGO [3] pointed to the existence of a local magnetic field  $H_{loc}$  of the order of 20–30 G in this compound. This field originates from the electronic system of the crystal because it consider-

ably exceeds the nuclear local magnetic fields (several G), although is inferior to  $H_{loc}$  in conventional magnets comprising atoms with unfilled  $d$ - or  $f$ -electron shells ( $10^3$ – $10^6$  G). In weak (below 500 Oe) constant external magnetic fields  $H_{ext}$ , the spin echo intensity in the  $^{209}\text{Bi}$  NQR spectrum of BGO increased dramatically (by about an order of magnitude) [2]. Such behavior was shown to correlate with the spin dynamics features: in  $H_{ext}$ , the effective time  $T_2^*$  of nuclear quadrupole spin–spin relaxation markedly extended [3, 4]. This resulted in the fourfold increase in the spin echo amplitude even in the fields as small as  $H_{ext} \sim 15$  Oe at the pulse separation  $\Delta\tau \sim 125 \mu\text{s}$  [3, 4]. This finding stimulated a spin dynamics study on the BGO single

\*E-mail: orlov@mbslab.kiae.ru

crystal doped with the “magnetic” atoms of transition or rare earth elements. It was shown that even minor amounts (several tenths of mol%) of Cr, Pr, Nd, and Gd atoms inserted into the samples resulted in a strong (up to the 8-fold) elongation of the SEE decay (increase in  $T_2^*$ ), whereas the values of the quadrupole coupling constant  $e^2Qq_{zz}/h$  and the EFG asymmetry parameter  $\eta$  at the Bi nucleus remained unchanged [4]. We note that normally, the insertion of paramagnetic atoms shortens  $T_2^*$ , acting as an additional source of relaxation. For compounds of the specified type, this result pointed to the doping as a procedure for increasing the spin–spin relaxation time  $T_2^*$ , which is an important time scale in quantum computing and spintronics characterizing the spin phase decoherence time. The elongation of the decoherence time is one of the crucial problems in both mentioned fields.

Naturally, the question of the influence of paramagnetic dopants on the nuclear spin–lattice relaxation in the BGO crystal was also interesting. A flattened minimum, found between 5–7 K by carefully studying the temperature dependence of the spin–lattice relaxation rate  $T_1^{-1}$  in a nondoped BGO crystal, was understood as a direct evidence for the existence of the paramagnetic centers in BGO [5]. An examination of the contribution of such centers to the spin–lattice relaxation rate and evaluation of the characteristic extent of splitting of their electron levels ( $\Delta \sim 35\text{--}40$  K) in the BGO crystal electric field (CEF) enabled us to suggest that these centers are the holes in the  $p$ -electron shell of the oxygen atoms [5]. In this paper, the results of a study of the spin–lattice relaxation time  $T_1$  vs. temperature are presented for BGO crystals doped with the Cr (0.015 mol%), Gd (0.2 mol%), and Nd (0.5 mol%) atoms.

## 2. EXPERIMENTAL

The  $^{209}\text{Bi}$  nuclear spin–lattice relaxation time in the doped  $\text{Bi}_4\text{Ge}_3\text{O}_{12}$  single crystals was measured between 4.2–300 K using a home-built pulse NQR spectrometer based on Matec gated amplifier 515A and 525 which operates in the range 2–60 MHz. The values of  $T_1$  were determined from the amplitude of echo signals observed after the pulse sequence  $180^\circ - \tau - 90^\circ - \tau_e - 180^\circ$  (the inversion–recover procedure) for the  $\Delta m = 1/2 - 3/2$  and  $\Delta m = 3/2 - 5/2$  transitions in the  $^{209}\text{Bi}$  NQR spectrum of  $\text{Bi}_4\text{Ge}_3\text{O}_{12}$ . The nondoped single crystal of  $\text{Bi}_4\text{Ge}_3\text{O}_{12}$  was grown as described in Ref. [2]. The doped crystals were prepared by mixing  $\text{Bi}_2\text{O}_3$  and  $\text{GeO}_2$  with the appropriate amount of  $\text{M}_2\text{O}_3$  ( $\text{M} = \text{Cr}$ ,

Nd, Gd) powder followed by growing a sample in Pt crucibles according to the Czochralski method. The raw materials contained less than  $10^{-6}$  mass% of impurities.

## 3. RESULTS AND DISCUSSION

As was shown previously, the nuclear quadrupole spin–lattice relaxation for the nucleus with spin  $I = 9/2$  can be adequately described by the single effective spin–lattice relaxation time  $T_1^*$  for each of the four quadrupole transitions ( $\Delta m = 1/2 - 3/2, \dots, 7/2 - 9/2$ ) instead of the four relaxation times  $T_{1i}$  ( $i = 1, 2, 3, 4$ ) [6].

Figure 1 shows the measured and modeled curves of the temperature dependence of the spin–lattice relaxation time  $T_1^*$  for the transition  $\Delta m = 3/2 - 5/2$  in the  $^{209}\text{Bi}$  NQR spectrum of the nondoped and doped BGO crystals. It can be seen that near room temperature,  $T_1^*$  markedly shortens as the temperature increases, the relaxation mechanism being mainly related to lattice motions. In this temperature region, the  $T_1^*$  values for all the samples differ insignificantly.

Near 4.2 K, the lattice contributions to the relaxation process become negligible, and notable contribution into  $T_1^*$  from the interaction of nuclear spins with paramagnetic centers is observed for all the samples including the nondoped BGO, the  $T_1^*$  values for it considerably (by 2–3 orders of magnitude) exceeding those for the doped samples.

In the temperature range from 4.2 to 77 K, all the samples studied exhibit an essentially different behavior of  $T_1^*$  with temperature. For the nondoped crystal, the curve  $T_1^*(t)$  shows a flattened maximum between 5–7 K [5]. The curve  $T_1^*(t)$  for the Nd-doped sample shows a distinctive maximum in the range 30–40 K, which is shown below to originate from the CEF effect. Near 4.2 K, this curve approaches a constant. For the Gd-doped crystal, the curve  $T_1^*(t)$  is virtually independent of temperature due to the absence of the CEF effects. It reveals a notable contribution to the spin–lattice relaxation of the electron mechanism based on the temperature-independent electron spin-flip process [7].

Although the temperature behaviors of the curves in Fig. 1 differ from each other, their basic features at low temperatures can be described using the formulas used previously for the analysis of the spin–lattice relaxation rate in the nondoped BGO:

$$T_1^{-1} = (T_1^{-1})_e + (T_1^{-1})_l. \quad (1)$$

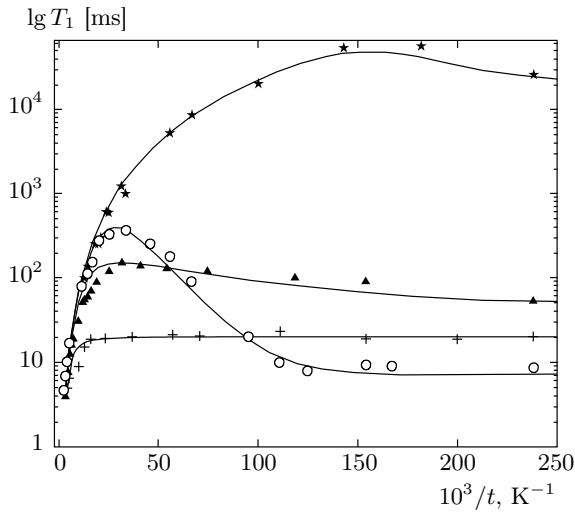


**Fig. 1.** Temperature dependence of the nuclear spin-lattice relaxation time for the transition  $\Delta m = 3/2 - 5/2$  in the  $^{209}\text{Bi}$  NQR spectrum of the BGO crystals. The measured data:  $\star$  — nondoped,  $\circ$  — doped with Nd,  $\blacktriangle$  — doped with Cr,  $+$  — doped with Gd; solid lines are the modeled curves

The second term in (1) is the contribution of the lattice vibrations, which was taken in [5] in the form

$$(T_1^{-1})_l = bt^n. \quad (2)$$

The values of  $b = 1.5 \cdot 10^{-4} \text{ s}^{-1}/\text{K}^n$  and  $n = 2.5$  found from the high-temperature part of  $T_1^*(t)$  [5], are used in what follows for the analysis of all the curves in Fig. 1 assuming that small amounts of paramagnetic dopants do not affect the lattice properties of doped BGO single crystals.

As can be seen from Fig. 1, the rate of relaxation at the intrinsic paramagnetic centers, which are the holes in the  $p$ -electron shells of the oxygen atoms [5], is 2–3 orders of magnitude lower than the rate caused by  $f$  or  $d$  electrons of the dopant atoms. Hence, for the doped BGO crystals, we take only the electron contribution of paramagnetic centers into account in the first term of (1) [8]:

$$(T_1^{-1})_e = K\tau_e, \quad (3)$$

where  $\tau_e$  is the correlation time for the electron spin of the dopant atom and  $K$ , as in [5], is an adjustable parameter. Similarly, the electron spin correlation time  $\tau_e$  is the sum of the contributions,

$$\tau_e^{-1} = T_{1e}^{-1} + \tau_s^{-1}, \quad (4)$$

where  $\tau_s$  is the temperature-independent characteristic time of the electron spin flip [7] and  $T_{1e}$  is the spin-

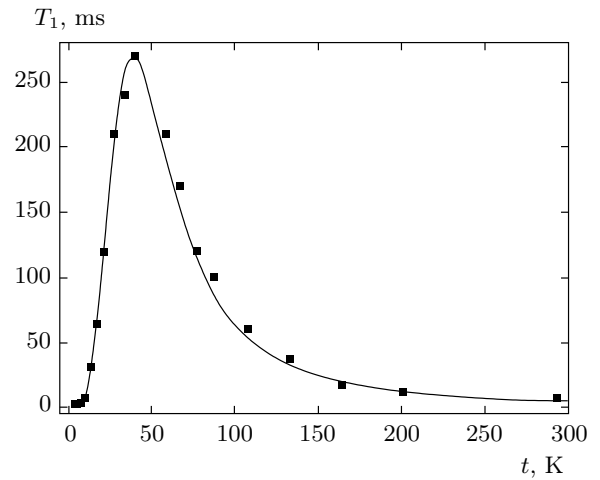


**Fig. 2.** Temperature dependence of the nuclear spin-lattice relaxation time for the transition  $\Delta m = 1/2 - 3/2$  in the  $^{209}\text{Bi}$  NQR spectrum of the Nd-doped BGO crystal:  $\blacksquare$  — the measured data; the solid line is modeled using the parameters in Table

lattice relaxation time of the electron spins of the paramagnetic center,

$$T_{1e} = ae^{\Delta/t}. \quad (5)$$

In (5),  $a$  is an adjustable parameter,  $\Delta$  is the space between the ground level and the first excited electron level of the paramagnetic center split by the CEF. The analysis of the measured curves  $T_1^*(t)$  using the above formulas gives the parameter values for  $\text{Bi}_4\text{Ge}_3\text{O}_{12}$  listed in Table.

The solid lines in Fig. 1 were calculated using formulas (1)–(5) and the appropriate values of the parameters in Table. Figure 2 shows the measured data and the modeled curve for the Nd-doped BGO crystal in linear axes.

The parameter  $\Delta$  for the Nd-doped BGO crystal can be evaluated from the known  $^{209}\text{Bi}$  NQR data for BGO [2] and the crystal potential model [9]. The Hamiltonian of interaction between the CEF and the nuclear electric quadrupole moment for the CEF of single-axis symmetry is

$$\hat{H}_Q = \frac{QeV_{zz}(1-\gamma)}{4I(2I-1)} [3I_z^2 - I(I+1)], \quad (6)$$

where  $Q$  is the nuclear electric quadrupole moment,  $I$  is the nuclear spin,  $z$  is the principal axis of the EFG tensor for the CEF,  $V_{zz}$  is the  $z$ -component of the EFG tensor, and  $\gamma$  is the Sternheimer antishielding factor [10]. As follows from the crystal potential model [9],

**Table.** The values of parameters in formulas (2)–(5) that gave the best agreement with the measured data

BGO single crystal	Transition	$\Delta$ , K	$Ka$ , s <sup>-1</sup>	$K\tau_s$ , s <sup>-1</sup>
Nondoped	$\Delta m = 1/2 - 3/2$	$40 \pm 5$	$(0.5 \pm 0.1) \cdot 10^{-5}$	$0.025 \pm 0.005$
	$\Delta m = 3/2 - 5/2$	$40 \pm 5$ [5]	$(1.5 \pm 0.5) \cdot 10^{-5}$ [5]	$0.045 \pm 0.01$ [5]
Doped with Nd (0.5 mol%)	$\Delta m = 1/2 - 3/2$	$60 \pm 10$	$0.48 \pm 0.05$	$450 \pm 50$
	$\Delta m = 3/2 - 5/2$	$60 \pm 10$	$0.28 \pm 0.05$	$140 \pm 10$
Doped with Gd (0.2 mol%)	$\Delta m = 1/2 - 3/2$	–	–	$100 \pm 20$
	$\Delta m = 3/2 - 5/2$	–	–	$50 \pm 10$
Doped with Cr (0.015 mol%)	$\Delta m = 1/2 - 3/2$	$15 \pm 2$	$11.5 \pm 0.5$	$14 \pm 0.5$
	$\Delta m = 3/2 - 5/2$	$15 \pm 2$	$5.0 \pm 0.2$	$21 \pm 2$

apart from the expression for quadrupole Hamiltonian (6),  $V_{zz}$  enters the expression for the coefficient

$$B_2^0 = -e \frac{V_{zz}}{4} \langle r^2 \rangle (1 - \sigma_2) \alpha_J \quad (7)$$

of the Hamiltonian of interaction between the CEF and  $4f$  electrons of rare earth ions residing in the 3-fold axis (the principal diagonal of the cube) in the BGO crystal

$$\hat{H}_{CEF} = B_2^0 O_2^0 + B_4^0 O_4^0 + B_4^4 O_4^4 + B_6^0 O_6^0 + B_6^4 O_6^4. \quad (8)$$

In (7),  $\langle r^2 \rangle$  is the mean squared radius of the  $4f$  electron. For the  $\text{Nd}^{3+}$  ion,  $\langle r^2 \rangle \approx 1a_B^2$  [11],  $\sigma_2$  is the Sternheimer shielding factor. For  $\text{Nd}^{3+}$ , no theoretical value of  $\sigma_2$  is known to the authors, but for the neighboring  $\text{Pr}^{3+}$ ,  $\sigma_2 = 0.67$  [12], and we therefore used  $\sigma_2 = 0.6$  for  $\text{Nd}^{3+}$ .

The values of numerical coefficients  $\alpha_J$  are known for the ground state of all the rare earth ions [13], that for the  $\text{Nd}^{3+}$  ion being  $\alpha_J = -7/(9 \cdot 121)$ . Therefore, the magnitude of  $V_{zz}$  is to be known for the evaluation of the coefficient  $B_2^0$  in (7). This can be derived from the value of the  $^{209}\text{Bi}$  quadrupole coupling constant for BGO, which is  $q = 490.3$  MHz [2]:

$$q = \frac{QeV_{zz}(1 - \gamma)}{h}. \quad (9)$$

The values of both  $Q$  and  $\gamma$  in (9) are known from the literature:  $Q = -0.4 \cdot 10^{-24}$  cm<sup>2</sup> [14] and  $\gamma = -60.78$  [15]. The latter was calculated for the  $\text{Bi}^{3+}$  ion using the relativistic Hartree–Fock–Slater method. From (7) and (8) one can evaluate the coefficient  $B_2^0$  is  $B_2^0 \approx 1.5$  meV. Because the other coefficients in CEF Hamiltonian (8) are presently unknown, we use only the first term in (8) for the estimation of the CEF effects, where the operator  $O_2^0 = 3J_z^2 - J(J+1)$  and the quantum number  $J$  of the total moment of the  $\text{Nd}^{3+}$

ion  $4f$ -shell is  $J = 9/2$ . Using the standard procedure for finding the eigenvalues and eigenfunctions of Hamiltonian (8), we can evaluate the splitting  $\Delta$  between the ground  $|\pm 1/2\rangle$  and first excited level  $|\pm 3/2\rangle$  for  $4f$  electrons of the  $\text{Nd}^{3+}$  ion to be 9 meV = 104 K, which is consistent by the order of magnitude with  $\Delta = 60$  K given in Table. This confirms the above suggestion that the maxima on the curves  $T_1^*(t)$  between 4.2 and 77 K originate from the CEF effects.

The  $\text{Nd}^{3+}$  and  $\text{Gd}^{3+}$  ions are isovalent to  $\text{Bi}^{3+}$  and seem to replace them in the BGO lattice residing in the threefold axis (the cube principal diagonal). As a result, the ground  $^4I_{9/2}$  multiplet of the  $4f$ -electron shell, which has the  $4f^3$  configuration in the  $\text{Nd}^{3+}$  ion, is split into 5 doublets by the BGO CEF of tetragonal symmetry (the space group  $I43d$  or  $T_d^6$  [16]). The splitting extent  $\Delta$  between the ground and first excited levels of the  $^4I_{9/2}$  multiplet is one of the basic parameters that determine the electron contribution to  $T_1^*(t)$  and may be found from the measured data.

The  $4f^7$  configuration of the  $\text{Gd}^{3+}$  ion  $f$ -electron shell signifies the zero  $4f$ -shell total orbital moment. If  $^8S_{7/2}$  is the ground state of the  $\text{Gd}^{3+}$  ions, then both the CEF effects and the intermultiplet splitting of the ground spectroscopic term are absent in the first approximation. This causes a marked difference in the  $T_1^*(t)$  behavior of the Nd- and Gd-doped samples.

The  $\text{Cr}^{3+}$  and  $\text{Cr}^{4+}$  ions of the  $3d^3$  and  $3d^2$  configurations respectively have the ground spectroscopic states  $^4F_{3/2}$  and  $^3F_2$ , which permits the splitting of the  $3d$ -electron levels in the tetragonal CEF into two doublets in the former, and a singlet and two doublets in the latter case. Thus, for the Cr-doped sample of BGO, the CEF effects are expected to make a contribution to the nuclear spin–lattice relaxation between 4.2 K and room temperature.

The samples prepared can therefore yield a fairly complete picture of CEF contributions into the temperature dependence of the nuclear spin–lattice relaxation.

From the standpoint of the CEF theory, the effect of the CEF on the  $\text{Nd}^{3+}$   $4f$  electrons in BGO may be to a first approximation considered to be weak with respect to the spin–orbit interaction

$$\hat{H}_{LS} = \lambda \mathbf{L} \cdot \mathbf{S}, \quad (10)$$

which produces the intermultiplet splitting. This is because the estimation of the complete splitting of the  $\text{Nd}^{3+}$  ion multiplet  ${}^4I_{9/2}$  from the first term in Hamiltonian (8) gave the value of the order of 1000 K, which is about 2.5 times smaller than the distance between the ground and first excited multiplet  ${}^4I_{11/2}$  of the  $\text{Nd}^{3+}$  ion.

For the chromium  $3d$  electrons, the CEF effects in the appropriate BGO sample seem to be of the same order as the spin–orbit interaction. Therefore, in a free  $\text{Cr}^{3+}$  ion, the constant  $\lambda = 87 \text{ cm}^{-1} = 10.8 \text{ meV}$  [17], and the evaluation of  $\Delta$  for the  ${}^4F_{3/2}$  and  ${}^3F_2$  states of the  $\text{Cr}^{3+}$  and  $\text{Cr}^{4+}$  ions is difficult because of the lack of information on the  $B_4^0$  and  $B_4^4$  coefficients for the Hamiltonian in the  $|ls\rangle$  representation

$$\hat{H} = B_2^0 O_2^0 + B_4^0 O_4^0 + B_4^4 O_4^4 + \zeta \hat{\mathbf{L}} \cdot \hat{\mathbf{S}}, \quad (11)$$

with the constant  $\zeta = \lambda \cdot 2S$  [17]. Considering the relatively small value of the adjustable parameter  $\Delta = 15 \text{ K}$  for the chromium ions (see Table), we have to admit that the coefficients  $B_4^0$  and  $B_4^4$  in (11) are important for finding the true scheme of the  $3d$ -electron levels in the BGO CEF.

#### 4. CONCLUSIONS

Minute amounts of paramagnetic dopants (the tenth and even hundredth fractions of mol%) in the BGO single crystal strongly accelerate the nuclear quadrupole  ${}^{209}\text{Bi}$  spin–lattice relaxation below 77 K. Thus, at 4.2 K, when the contribution to the nuclear spin–lattice relaxation from the electrons of paramagnetic centers becomes predominant, the effective spin–lattice relaxation time  $T_1^*$  for the nondoped BGO single crystal is 2–3 orders of magnitude longer than that for the BGO crystals doped with the Cr, Nd, and Gd atoms.

In the nondoped BGO single crystal, the presence of the intrinsic paramagnetic centers, which are the holes in the  $p$ -electron shells of the oxygen atoms, was clearly evidenced by the temperature dependence of the nuclear quadrupole spin–lattice relaxation.

For the doped BGO crystals, the CEF effects resulted in a nonmonotonic temperature dependence of

the effective spin–relaxation time  $T_1^*$  between 77 and 4.2 K.

Near room temperature, when the contribution of the lattice vibrations to the nuclear spin–lattice relaxation is prevailing, the values of  $T_1^*$  for both doped and nondoped BGO samples were similar. We note that the same BGO samples demonstrated a dramatic (8-fold) increase in the effective nuclear spin–spin relaxation time upon doping [4].

V. G. O. and G. S. S. appreciate the financial support from the program Higher School Scientific Potential Development grant № 2.1.1./4540. E. A. K. is grateful to the Presidium of RAS (Program № 20) for financial support.

#### REFERENCES

1. E. A. Kravchenko, V. G. Orlov, and M. P. Shlykov, *Russian Chem. Rev.* **75**, 77 (2006).
2. E. A. Kravchenko, Yu. F. Kargin, V. G. Orlov et al., *J. Magn. Magn. Mater.* **224**, 249 (2001).
3. E. A. Kravchenko, V. G. Orlov, V. G. Morgunov et al., *Hyperfine Interact.* **176–181**, 437 (2008).
4. E. A. Kravchenko, V. G. Morgunov, V. G. Orlov et al., *JETP Lett.* **86**, 337 (2008).
5. E. A. Kravchenko, Tetsuo Asaji, V. G. Orlov et al., *Sol. St. Comm.* **148**, 319 (2008).
6. A. A. Gippius, D. F. Khozeev, E. N. Morozova et al., *J. Phys.: Condens. Matter* **14**, 3891 (2002).
7. A. Birkeland and I. Svare, *Phys. Scrip.* **18**, 154 (1978).
8. A. Abragam, *The Principles of Nuclear Magnetism*, Clarendon, Oxford (1961).
9. V. G. Orlov, *J. Magn. Magn. Mater.* **61**, 337 (1986).
10. R. M. Sternheimer, *Phys. Rev.* **80**, 102 (1950).
11. A. J. Freeman and R. E. Watson, *Phys. Rev.* **127**, 2058 (1962).
12. P. Erdos and J. H. Kang, *Phys. Rev. B* **6**, 3393 (1972).
13. V. N. Hutchings, *Sol. St. Phys.* **16**, 227 (1964).
14. A. Lösche, *Kerninduktion*, Veb Deutscher Verlag der Wissenschaften, Berlin (1957).
15. F. D. Feiock and W. R. Johnson, *Phys. Rev.* **187**, 39 (1969).
16. S. F. Radaev, L. A. Muradyan, Yu. F. Kargin et al., *Kristallografia* **35**, 361 (1990) (*Sov. Phys. Krystallogr.* **35**, 204 (1990)).
17. S. A. Al'tshuler and B. M. Kozyrev, *Electronic Paramagnetic Resonance of Compounds of Intermediate Group Elements*, Nauka, Moscow (1972) (in Russian).